NASA/CR—2003–212504

Modeling Charge Collection in Detector Arrays

J.C. Pickel
PR&T, Inc., Bonsall, California

Prepared for Marshall Space Flight Center
Under H-Order 32491D
and sponsored by
The Space Environments and Effects Program
managed at the Marshall Space Flight Center

June 2003

The NASA STI Program Office…in Profile

Since its founding, NASA has been dedicated to the advancement of aeronautics and space science. The NASA Scientific and Technical Information (STI) Program Office plays a key part in helping NASA maintain this important role.

The NASA STI Program Office is operated by Langley Research Center, the lead center for NASA's scientific and technical information. The NASA STI Program Office provides access to the NASA STI Database, the largest collection of aeronautical and space science STI in the world. The Program Office is also NASA's institutional mechanism for disseminating the results of its research and development activities. These results are published by NASA in the NASA STI Report Series, which includes the following report types:

- TECHNICAL PUBLICATION. Reports of completed research or a major significant phase of research that present the results of NASA programs and include extensive data or theoretical analysis. Includes compilations of significant scientific and technical data and information deemed to be of continuing reference value. NASA's counterpart of peer-reviewed formal professional papers but has less stringent limitations on manuscript length and extent of graphic presentations.

- TECHNICAL MEMORANDUM. Scientific and technical findings that are preliminary or of specialized interest, e.g., quick release reports, working papers, and bibliographies that contain minimal annotation. Does not contain extensive analysis.

- CONTRACTOR REPORT. Scientific and technical findings by NASA-sponsored contractors and grantees.

- CONFERENCE PUBLICATION. Collected papers from scientific and technical conferences, symposia, seminars, or other meetings sponsored or cosponsored by NASA.

- SPECIAL PUBLICATION. Scientific, technical, or historical information from NASA programs, projects, and mission, often concerned with subjects having substantial public interest.

- TECHNICAL TRANSLATION. English-language translations of foreign scientific and technical material pertinent to NASA's mission.

Specialized services that complement the STI Program Office's diverse offerings include creating custom thesauri, building customized databases, organizing and publishing research results…even providing videos.

For more information about the NASA STI Program Office, see the following:

- Access the NASA STI Program Home Page at ***http://www.sti.nasa.gov***

- E-mail your question via the Internet to help@sti.nasa.gov

- Fax your question to the NASA Access Help Desk at (301) 621–0134

- Telephone the NASA Access Help Desk at (301) 621–0390

- Write to:
  NASA Access Help Desk
  NASA Center for AeroSpace Information
  7121 Standard Drive
  Hanover, MD 21076–1320
  (301)621–0390

NASA/CR—2003–212504

Modeling Charge Collection in Detector Arrays

J.C. Pickel
PR&T, Inc., Bonsall, California

Prepared for Marshall Space Flight Center
Under H-Order 32491D
and sponsored by
The Space Environments and Effects Program
managed at the Marshall Space Flight Center

National Aeronautics and
Space Administration

Marshall Space Flight Center • MSFC, Alabama 35812

June 2003

Acknowledgments

This effort was accomplished with resources provided by NASA's Living With a Star (LWS) Space Environment Testbeds (SET) Program.

Available from:

NASA Center for AeroSpace Information
7121 Standard Drive
Hanover, MD 21076–1320
(301) 621–0390

National Technical Information Service
5285 Port Royal Road
Springfield, VA 22161
(703) 487–4650

EXECUTIVE SUMMARY

High fidelity prediction of ionizing particle effects in space-based optical sensors is important for optimized designs. Predictions require transport of the external radiation environment to the detector arrays and then detailed modeling of the transport of radiation-induced charge to individual pixels. A modeling approach is described for predicting charge collection in space-based infrared detector arrays due to ionizing particle radiation. The modeling uses a combination of analytical and Monte Carlo techniques to capture the essential features of energetic-ion-induced charge collection to detector pixels in a two-dimensional large format array. The model addresses several aspects that are important for high fidelity simulation of complex focal plane array structures including: multiple layers, sub-regions within layers, variation of linear energy transfer with particle range, secondary electron scattering, free-field diffusion, and field-assisted diffusion. The models are implemented in code and developed as an engineering tool for assessment of single particle effects on arrays of charge collecting elements.

The device geometry is described by pixel pitch and layers (e.g., detector, ROIC, indium bump) on a Cartesian coordinate system. Depletion region and diffusion region thicknesses are defined and the boundary of regions within the pixel are defined. A particle is incident on the top surface of the device with a random location and random angle of incidence. The particle type and energy determine the linear energy transfer (LET). A subarray (11 pixels x 11 pixels) is defined around the hit pixel. The primary particle traverses through the layers in a straight path along the trajectory and the appropriate charge collection model is applied, depending on the type of region – either depletion (high electric field), diffusion (low electric field), drift/diffusion (moderate electric field), or recombination (dead layer or recombination surface). Diffusion length is limited by recombination lifetime. The charge generated along the particle path is partitioned to the appropriate pixels in the subarray. The process is repeated for a large number of particle hits and the subarray results for each hit are accumulated in a large array (100 pixels x 100 pixels). A noise model is used to generate a noise floor that is added to the data across the array. The large array is of sufficient size to capture all of the statistical features of the interactions. A larger image can be built up from stitching together multiple 100x100 arrays. The model is coded in Visual Basic and integrated with Microsoft Excel. The code has a Windows-based graphical user interface. The code is named REACT (Radiation Environment Array Charge Transport).

This work is of specific significance for design of sensor missions that are concerned with noise levels of FPAs operated in the space environment, and of general significance for studying particle-induced charge collection in two-dimensional arrays of integrated circuits. The array modeling and engineering software tools that were developed can be used to plan mitigation schemes for ionizing particle radiation on space missions before the sensors are designed, built and launched. In addition, the Monte Carlo model of transport of ionizing radiation created carriers in integrated circuits with varying electric fields and varying lifetime regions will have broader application to all charge collection problems associated with single event effects (SEE). Example results are given and predictions are compared to experimental data.

TABLE OF CONTENTS

LIST OF FIGURES

LIST OF FIGURES (Continued)

LIST OF TABLES

1. Introduction

This is the final report for NASA Order #H-32491D issued under NRA 8-31. The contract was managed by NASA Marshall Space Flight Center with Ms. Donna Hardage as COTR. The period of performance was December 21, 2001 to December 20, 2002. The report is organized as follows: After a statement of objectives and scope, some background discussion is given for the requirements and applications of the modeling tools that were developed. The ionizing particle environment for space-based sensors is described. The modeling approach is reviewed with discussion of the various assumptions and simplifications. Several practical considerations for implementing the modeling in code for large format arrays are discussed. Charge collection processes are discussed for drift in high electric field regions, diffusion in low field regions and drift-assisted diffusion in moderate field regions. The models that are used to describe the charge collection processes and the algorithms used to implement the procedures in code are given, along with example results. A discussion of the code flow and major program modules is provided. Typical results are provided and approaches for calibration of model parameters based on experimental data are discussed.

The modeling approach was presented at the 2002 Single Event Effects Symposium, at the 2002 IEEE Nuclear and Space Radiation Effects Conference (NSREC), and accepted for publication in the IEEE Transactions on Nuclear Science [1].

2. Objectives and Scope

The objective of this work was to develop and validate a detector array charge collection model that can be used as an engineering tool to aid in the design of optical sensor missions for operation in the space radiation environment. The scope of this work was enhancement of the prototype array charge collection model that was developed for the James Webb Space Telescope (JWST) program. Transport of the external particle environment through the surrounding material to the focal plane array (FPA), and low energy electron and other particle transport within the FPA, is being done on the JWST program. The primary enhancements to the prototype array charge transport model were accounting for drift-assisted diffusion by Monte Carlo modeling techniques and implementing the modeling approaches in a windows-based code. The modeling is concerned with integrated charge collection within discrete pixels in the FPA, with high fidelity spatial resolution. Temporal effects are not included. The modeling is applicable to all detector geometries including monolithic CCDs, Active Pixel Sensors (APS) and hybrid FPA geometries based on a detector array bump-bonded to a ROIC.

3. Background

Optical sensors for space-based imaging missions have evolved toward large format two-dimensional arrays of detectors. Significant advances have been made in infrared (IR) detector array and readout integrated circuit (ROIC) technology, with greatly improved sensitivity and reduced noise levels. It is not uncommon to see read noise specifications on the order of 10 electrons or less, concomitant with very long integration times of several hundred to thousands of seconds [2]. With these performance

very long integration times of several hundred to thousands of seconds [2]. With these performance requirements and operation in space, the radiation environment from galactic cosmic rays (GCR), trapped particles and energetic solar particles can dominate the noise in the focal plane array (FPA) pixels [3]. Optical detectors, by design, are efficient sensors of ionization and the single event transients from energetic particles in the space environment are registered in the FPA pixels when they are penetrated by the particles. Shielding is not effective due to the high energies of the particles and because of secondary particle generation when passing through shielding. The particle-induced noise can be mitigated through a variety of signal processing techniques and operational scenarios. For mitigation strategies to be successful, it is necessary to have a high-fidelity predictive model of the charge collection in the detector arrays, particularly the spatial distribution of the particle-induced charge. The problem has become more challenging as the noise levels have been reduced with modern technology and enhanced performance requirements.

Charge generated from single event transients is captured on the integration nodes of detector array pixels and remains until the array is reset at the end of the integration time. The very low noise floor of a few electrons in modern detector arrays implies that essentially every primary particle and every secondary particle that reaches the sensitive volume of the FPA contaminates the pixels with noise charge. For example, a noise floor of 10 electrons implies that only 10 eV of energy deposition is required to generate a charge pulse equal to the noise in near-IR detectors such as HgCdTe or InSb that have ionization energies of around 1 eV/e. Since characteristic pathlengths are on the order of 10 μm, a particle with linear energy transfer of only 1 eV/μm is problematic. The small noise charges that are near the noise floor cannot be removed by signal processing.

Imaging arrays typically have non-destructive readout capability. That is, the signal charge can be sampled multiple times during the integration time without disturbing the integrated charge. This fact enables signal processing algorithms to recognize and remove the charge-contaminated pixels that have suffered a particle transient.

For example, the science mission for JWST includes high resolution imaging and spectroscopy in a near infrared (NIR) wavelength band with cut-off wavelength of ~5 μm, and a mid infrared (MIR) band with cut-off wavelength of ~28 μm. The requirements include a combination of very low noise (10 electrons or less) and very long integration times (hundreds to thousands of seconds). These requirements place unprecedented demands on performance with respect to transient radiation effects from the space environment. A preliminary estimate is that one practical limit to signal integration times will be about 1000 seconds, set by the primary cosmic ray flux. Longer exposure time may be possible using more sophisticated cosmic ray rejection software to identify hits and continue the integration [4]. Although this approach has worked well with other space-based observatories such as Near Infrared Camera Multi Object Spectrometer (NICMOS), it has not yet been empirically demonstrated at the noise levels required for JWST. Design of rejection schemes and mission planning for effective mitigation of the cosmic ray induced noise requires a priori knowledge of the FPA response to the total particle environment, including primary, secondary and radioactive decay particles.

The overall transient noise problem for an optical sensor in the space environment is illustrated in Fig. 1, showing the FPA enclosed in surrounding material (packaging, telescope, spacecraft, etc.).

The ionizing particle environments of concern include galactic cosmic rays (GCR) and solar-particle-event (SPE) generated protons, heavy ions, and electrons. In addition, inherent and induced radioactive sources in the material surrounding the FPA are potential sources of ionizing particles. The primary GCR particle environment in space is fairly well understood [5]. Secondary particles include delta electrons and nuclear reaction by-products.

The penetrating radiation through the spacecraft causes the structure to become radioactive by inducing nuclear reactions. The population of activated radioactive products will build up over the duration of the mission. There will be increased activation during and after solar particle events. In addition, inherent radioactive impurities contained in spacecraft materials are a source of ionization transients.

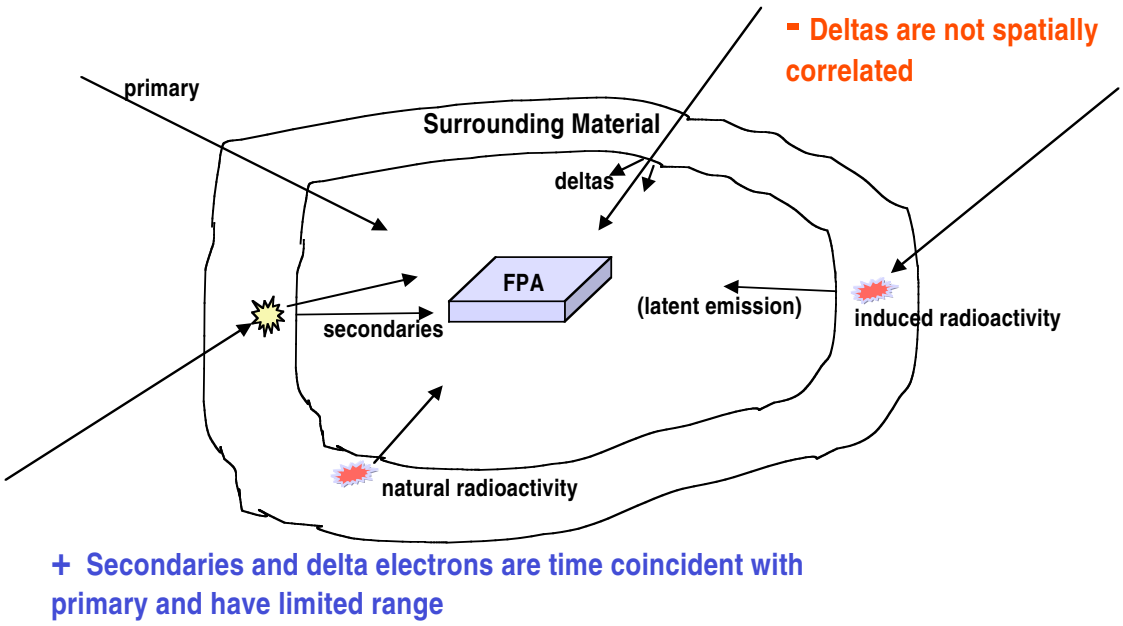

Figure 1. Ionizing particle radiation incident on the FPA.

There is field evidence of secondary particles interfering with IR telescopes from the on-orbit experience of the European Space Agency's Infrared Space Observatory (ISO) [6]. Measurement of transients in the ISO detectors indicated a transient rate approximately 80 % higher than could be accounted for by the primary particles. The higher than expected transient rate was attributed to secondary particles and delta electrons.

The external ionizing particle environment has been defined for the JWST program and Monte-Carlo transport analyses through typical spacecraft and surrounding structural material are underway to define typical ionizing particle environments at the location of the FPA. The Radiation Environment Array Charge Transport (REACT) code has been developed on this program to predict the spatially-dependent charge contamination of the FPA on a pixel-by-pixel basis. Both the detector layer and the readout integrated circuit layer in a hybrid FPA configuration are modeled. Incident particle events, both

primary and secondary, are characterized by the type of particle, energy, hit location on the surface of the FPA and angle of incidence. The charge generated in the FPA material is then distributed to the appropriate pixels to produce a pixel map of charge contamination events. The charge contamination pixel maps can be combined with pixel dark-field noise maps and imaging scenes to assess the performance impact. The modeling approach and engineering tools will allow predictions to be made for the effect of FPA transients under various scenarios including integration time, solar weather, FPA design and spacecraft design.

4.0 Modeling Approach

We seek a quantitative model for ionizing particle interaction with the FPA that will serve as an engineering tool for FPA design and mission planning. The goal of the modeling is to capture only the essential physics of the charge generation and collection, such that quantitatively accurate prediction can be made for charge contamination in the FPA pixels. Because integration times are long compared to charge collection times and charges are essentially "latched" into the pixel integration nodes until reset at the end of the integration period, the modeling does not address temporal effects. We assume that the local particle environment at the FPA is described by particle type, energy, hit location on the FPA and trajectory from a separate transport analysis (not the subject of this work).

The array charge transport modeling takes its basis from a similar approach used by Lomheim and co-workers to predict proton-induced charge deposits in charge coupled devices (CCDs) [7,8]. The model accounts for the spatial variation of charge collection in each pixel of the hybrid FPA following charge generation along the path of an ionizing particle, either electrons, protons or heavy ions. The model specifically addresses the 3-D geometry of charge collection volumes in a hybrid FPA, consisting of an array of detectors hybridized to a readout integrated circuit (ROIC) array through indium bump interconnects. Fig. 2 shows a cross-section of a typical hybrid FPA. Typical detector material for near-IR wavelengths would be HgCdTe or InSb. The substrate may be thinned or removed from the detector array to extend detection to shorter wavelength.

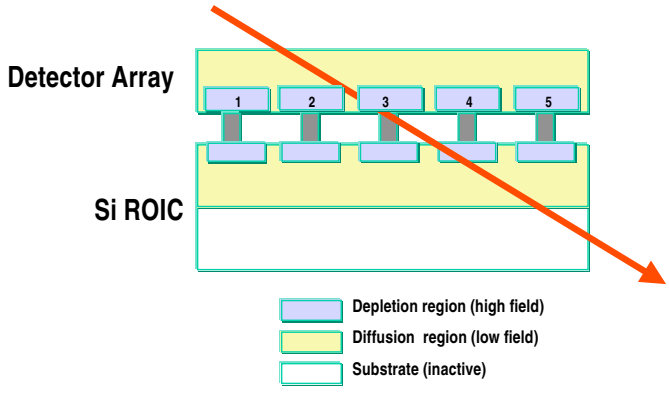

Figure 2. Typical hybrid IR FPA geometry. A detector array is hybridized to a Si ROIC through indium bump bonds. Charge collection due to the passage of ionizing particles occurs in both the detector array and the ROIC array.

The model output is a pixel map of charge deposits across the FPA due to the particles that strike the FPA during the integration time. This data can then be combined with a device-dependent distribution of inherent noise to produce a simulated "dark image" file.

The charge collection volumes (sensitive volumes) associated with a particular pixel are defined as those regions that collect charge to the integration capacitance for the pixel. The sensitive volumes in the photovoltaic detectors consist of the depletion volume of the p-n junction and the smaller of either a) the volume defined by the junction area and the minority carrier diffusion length in the detector active layer, or b) the pixel area and active layer thickness. The sensitive volumes in the ROIC are defined by the pixel pitch and the thickness of the Si epitaxial layer or the minority carrier diffusion length. Unless limited by wells or guardbands, the entire pixel volume of both the detector and the ROIC is sensitive to charge collection because the integration time is much longer than minority carrier lifetimes.

A key concern is charge spreading to adjacent pixels from the pixel that is penetrated by the particle, i.e., radiation transient crosstalk. Charge spreads by diffusion in both the detector array and the ROIC array. Mechanisms for charge spread by diffusion in the detector array are obvious since detector arrays are designed to collect photo-generated charge by diffusion from the active region with maximum efficiency. High density staring arrays typically do not have distinct charge separation barriers between the pixels. Instead, they rely on pixel geometry and slight electric fields from doping gradients to nudge the charge toward the local pixel junction. In all ROIC unit cells, a reset MOSFET is required to reset the integration capacitor and the junction that is connected to the integration capacitor is a sensitive charge collection junction. Charge collected on the sensitive junction is transported to the integration capacitor. The integration time is long compared to minority carrier diffusion times. Thus, all charge that diffuses from the ion path to any sensitive junction in the ROIC will be collected and counted to the respective pixel. In order to accurately model the charge collection by diffusion, the field-assisted drift component associated with the MOSFETs, and perhaps built-in fields in the diffusion regions of the detectors, needs to be taken into account. Similar considerations for charge spreading by diffusion apply to CCD, active pixel sensor (APS) and photovoltaic (PV) detector technologies.

The modeling task is to calculate charge generation along the 3-D path of the particle and follow the generated minority carriers until they are collected on a pixel integration node or recombine. For the current version of the model, we are not addressing temporal variation of charge collection since integration times are typically much longer than charge collection times. The final result is a spatial mapping of charge collection across the array during the integration time.

Fig. 3 illustrates the general approach taken in the array charge transport model. For illustration, only the depletion and free-field diffusion layers of the detector are shown. In the actual model, the depletion and diffusion layers are further subdivided into regions with offsets from the pixel edges representing junctions and wells, providing a fully 3-D description of the structure. In addition, spatially dependent electric fields may exist that require consideration for drift-assisted diffusion. Such a modeling approach can be applied to any detector structure, including hybrid FPAs, integrated active pixel sensors (APS) and CCDs, by registering the various layers on the Cartesian coordinate system and propagating the particle trajectory through the structure.

The radiation source terms for the charge collection model are derived from the external particle environment transported through the material surrounding the FPA. The output of the transport analysis

is a list of particles incident on the FPA during the integration time. The particles include both primary and secondary particles and are described with attributes as listed in Table 1.

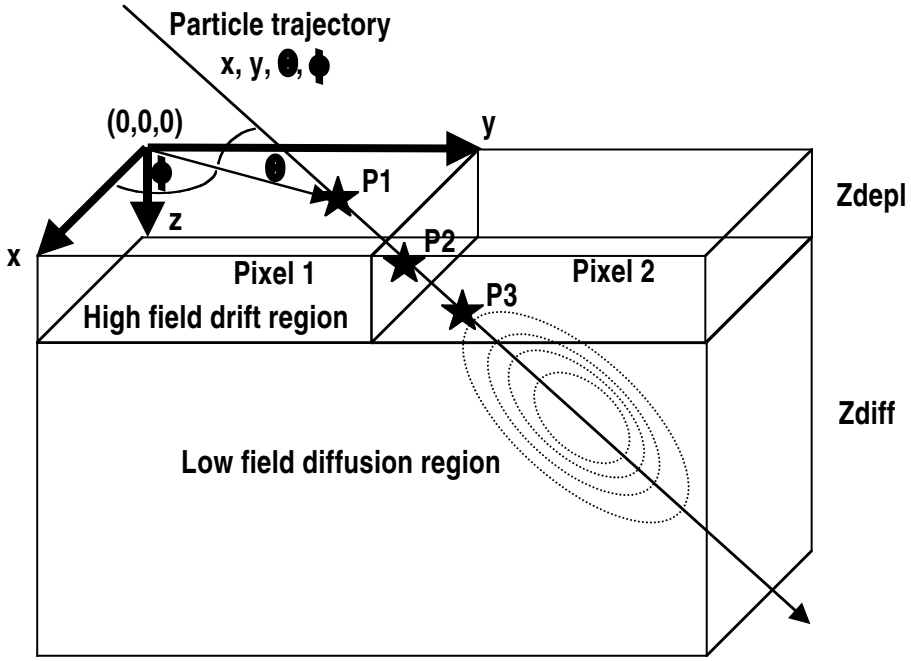

Figure 3. Simplified illustration of array charge transport model. A particle passes through depletion regions in pixel 1 from P1 to P2, and pixel 2 from P2 to P3 and then passes into the common substrate diffusion region.

Table 1. Incident Particle Attributes

Parameter	Symbol	Characteristics
Impact Position	X,Y	Random
Trajectory	_,_	Isotropic
Particle	Z,A	Depends on primaries, secondaries, radioactive decay
Energy	E	Conforms to energy spectrum at FPA after transport
Stopping Power	LET	Depends on Z, E
Range	R	Depends on Z,E

Table 2 lists the primary attributes of the FPA that determine the charge collection characteristics. The particle type and energy determine the linear energy transfer (LET). From the ionization energy for the target material, W, we determine the charge generation rate, linear charge deposition (LCD), in carriers/μm. Recombination of carriers is taken into account by assigning an effective diffusion length, L. As the particle loses energy to the target material, the energy decreases and the LET changes. The model accounts for this effect by recalculating the energy after each path increment based on the TRIM code [9].

Table 2. FPA Attributes

Parameter	Symbol	Characteristics
Material	InSb, HgCdTe or Si	Determines ionization: W, LCT
Pitch		Determines pixel geometry
Depletion Width and Pixel Offsets	Zdepl	Charge collection by drift
Diffusion Width and Pixel Offsets	Zdiff	Charge collection by diffusion
Spatially Variant Electric Field	E(r)	Charge collection by drift-assisted diffusion
Diffusion Length	Ldiff	Recombination-limited diffusion

4.1 Assumptions and Simplifications

The modeling goal is to determine the final spatial charge distribution across the array. Since noise levels on the order of 10 electrons are of concern, we are operating at levels much lower than are normally considered for radiation effects analysis. An exact accounting of the fate of each free carrier generated in a large format array (typically 2k x 2k pixels, or larger) during a long integration period is not computationally practical. Thus, we make several simplifying assumptions and utilize a combination of modeling approaches, including Monte Carlo techniques for particle hits and a combination of analytical and Monte Carlo solutions to charge collection.

The path of high energy protons and heavy ions is assumed to be a straight line through the FPA, defined as an array of detector pixels geometrically registered to an array of ROIC unit cells, with trajectory determined by the initial angle of incidence (_,_) and point of impact (x,y) on the surface. This assumption is justified since the ions are deviated from their path only by nuclear scattering and this is low probability in the small dimensions of the FPA.

However, the path of electrons is not straight. Their small mass can result in large angle scatters from collisions with bound electrons in the target material. To account for the zigzag path of the electrons, we use the Monte Carlo routines in the NOVICE code [10] and define a detour factor as the ratio of total pathlength to the practical range. For a range R, the energy deposition is then given by the product of R times the detour factor times the LET.

Each particle has a residual range that is determined by its energy. If a particle range is less than the remaining distance within the current pixel, the particle energy and resulting charge is assumed to be deposited at that point.

Energetic secondary electrons (delta electrons) are generated along the path of protons or heavy ions by Coulombic interactions that transfer energy to electrons in the target material. The delta electrons are a source of further ionization and charge deposition. We account for delta electron generation within the interior of the FPA assembly (active side of detector, interconnecting indium bump-bonds, and active side of ROIC) with a source generation function pre-calculated with the NOVICE code for each material of interest.

Secondary particle production from nuclear scattering is neglected since the probability is small within the small dimensions of the FPA.

Energy deposition is determined by LET and pathlength. LET is converted to LCD (e/um) by the ionization energy, W, for the target material. For HgCdTe and InSb with 5 μm cutoff wavelength, W is ~1.5 eV per carrier pair (eV/cp). For Si, W is ~3.7 eV/cp at cryogenic temperature.

4.2 Practical Considerations

Implementation of the analysis approaches described above into code with practical run times and reasonable computer resources requires consideration of several issues.

4.2.1 Subarray Windows

For a single particle interaction, it is neither practical nor necessary to consider charge collection from the entire array. Our approach was to define a small 11 pixel x 11 pixel subarray around the pixel initially penetrated by the particle. The hit is located within the center pixel (6,6) of the 11x11 subarray. The (x,y) location of the hit is maintained with respect to a larger 100x100 pixel array and with respect to the boundary of the center pixel in the subarray. After completion of all particles for a run, the hit subarray windows are located on the 100x100 array in the proper location. Overlap of subarrays is allowed with the total charge to the 100x100 array pixel accumulated from the overlapping subarray pixels.

4.2.2 Pixel Sub-regions

In some cases, it is necessary to consider subregions within a pixel that have different charge collection characteristics and require different modeling approaches. For example, the depletion region in the detector is often centered in the pixel and does not extend to the pixel edges. For ROIC pixels, both the depletion regions associated with junctions and the diffusion regions associated with wells are offset from the pixel edges. Our approach was to define subregions within a pixel and keep track of the region that the particle in as it travels along its trajectory. The appropriate charge collection model is applied depending on the region where the particle is currently located.

4.2.3 Multi-layers

Devices of interest often consist of multiple layers. For example, the hybrid FPA consists of 1) detector diffusion layer, 2) detector depletion layer, 3) dead layer, i.e., gap between detector and multiplexer, 4) multiplexer depletion layer and 5) multiplexer diffusion layer. The code allows for definition of multiple layers. As the particle traverses through the layers, the appropriate charge collection model is used for calculating the charge partitioning to the pixels in the vicinity.

4.2.4 LET Variation

As the particle loses energy along its path, the LET changes. For protons the change is negligible in typical path lengths through the device. However, for heavier ions, the effects are non-negligible, particularly for ground test environments where relatively low energy ions are used. The code accounts for the variation of LET along the particle path. The approach is to use tables of LET versus energy that are pre-computed from the TRIM code. For each path increment, the energy and LET are adjusted.

4.2.5 Incident Particle Environment

The particle environment incident of the array depends on the external environment and the shielding material surrounding the array. The environment is computed from a separate transport analysis and defined in a "hit file" that gives particle Z and energy. The code randomly selects a particle from the hit file and then randomly assigns a trajectory and a hit location on the array.

4.2.6 Secondary Electrons

Secondary electrons (deltas) that are incident on the charge collection regions generate charge. Generation of secondary electrons from the surrounding materials is performed in a separate analysis from the current code. The definition of the secondary electron environment is provided in a hit file that gives secondary electron energy and range. The code randomly selects a delta electron with a random hit location and trajectory. A precomputed detour factor is used to account for the zigzag path of the delta electron. The detour factor gives the ratio of the total path to the range.

5. Charge Collection

We are using a hybrid approach to charge collection. The initial line source of minority carrier distribution along the particle path depends on the particle LET, hit location (x,y) and trajectory (_,_). The final disposition of the carriers depends on the geometry and spatially-dependent minority carrier diffusion and drift. Particle history ends when it is either collected on a pixel node or recombination occurs. Charge collection is by drift, diffusion or a combination of drift and diffusion. We use different charge collection modeling approaches, depending on the local electric field in the current region along the pathlength.

5.1 Charge Collection by Drift

Charge generated within a high electric field region is transported by drift and we assume 100% collection efficiency to the associated pixel. High field collection regions could include depletion regions of p-n junctions in photovoltaic detectors or in ROIC junctions and high field region in impurity band conduction Si detectors. Charge collection in the depletion region is given by

$$Q_{depl} = LCD\ R_{depl} \quad (1)$$

where LCD is linear charge transfer (e/um), and R_{depl} is the pathlength in the depletion region.

5.2 Charge Collection by Diffusion

Charge generated in zero or low electric field regions is transported to the depletion/diffusion boundary by diffusion. Any charge that reaches the depletion/diffusion boundary is assumed to be collected on the associated pixel. We use an analytical solution to the 3-D diffusion equation that was developed by Kirkpatrick [11] to calculate the geometric distribution of charge to the pixel regions, similar to the approach used by Lomheim and coworkers [7,8]. The Kirkpatrick model solves the 3-D diffusion

equation for a point source, $Q_{ps}(x,y)$, at (x,y) coordinates on the depletion/diffusion interface plane. Boundary conditions assume a semi-infinite medium and recombination-limited diffusion length is not included. The result is

$$Q_{ps}(x,y) = LCD\ z' / 2\pi [(x - x')^2 + (y - y')^2 + (z - z')^2]^{3/2} \quad (2)$$

where x and y are coordinates at the depletion/diffusion boundary and x', y', z' are coordinates of a point source charge generator in the diffusion volume. $Q_{ps}(x,y)$ gives the charge per unit area at the depletion/diffusion boundary from a point source inside the diffusion region. $Q_{ps}(x,y)$ is integrated along the ion trajectory (_,_) for a chosen length, L, that determines the effective diffusion layer thickness and approximates the effects of recombination. This provides the surface charge density at the depletion/diffusion boundary due to a line source as

$$Q_{ls}(x,y,\_,\_,L) = (qn_0\cos(\_)/\pi k) [[(b\_+2a) / (a+b\_+\_^2)^{1/2}] - [(bL+2a) / (a+bL+L^2)^{1/2}]] \quad (3)$$

where

$a = x^2+y^2$
$b = -2(x\cos\Phi+y\sin\Phi)\sin\_$
$k = 4(x^2+y^2)-4(x\cos\Phi+y\sin\Phi)^2\sin^2\_$

and _ is an arbitrary small number to avoid a singularity at the proton entrance.

$Q_{ls}(x,y,\_,\_,L)$ is then numerically integrated over the pixel areas at the depletion/diffusion boundary to give the charge collected to each pixel (m,n) in the array as

$$Q_{diff}(m,n) = \iint Q_{ls}(x,y\ \_,\_,L)dxdy \quad (4)$$

We can account for spatially variant recombination-limited diffusion length by differencing the calculations along the trajectory and varying L appropriately.

5.3 Charge Collection by Field-Assisted Diffusion

The transport space is not uniform and some regions may have built-in fields due to doping gradients, variable fields due to device biasing, and spatial variation of minority carrier lifetime. For these intermediate field regions, we account for field-assisted diffusion. That is, the carriers will diffuse from their origin according to normal diffusion processes but there will be a drift bias that preferentially moves the diffusing charge cloud in the direction of the electric field. Here we use a hybrid Monte Carlo solution to the transport equation relating particle density to diffusion and drift.

We follow an approach first proposed by Sai-Halasz for simulating alpha particle single event effects in integrated circuits [12]. Rather than simulate the actual motion of the carriers, we simulate the simplest process that still follows, in average, the drift and diffusion processes described by the transport equation. A three-dimensional random walk is used with spatially dependent drift. For a diffusion length, L, a step, L_r, is randomly selected between –L and +L. Then the particle's x coordinate is

replaced by $x+L_r$. The same process is applied to the y and z coordinates and the cycle repeats for another particle.

Following Sai-Halasz, the time for the particle to move the random diffusion step, L_r , is given by

$$t_s = L_r^2 / 18\ D \tag{5}$$

where L_r is the diffusion step size and D is the diffusion coefficient.

If an electric field is present, a drift in the direction of the field will proceed concomitantly with the random diffusion step. The size of the drift step, $L_d(r)$, associated with each random diffusion step is given by the drift velocity and drift time, yielding

$$L_d(r) = (e\ E(r) / 18\ k\ T)\ L_r^2 \tag{6}$$

where T is temperature, k is Boltzmann's constant and E(r) is the local electric field. The total step is then given by $L_r + L_d$ and the appropriate step value is added to each dimension. The process repeats until the particle reaches either a collection surface such as a depletion region boundary, a recombination surface, a reflection surface, or until the lifetime-limited diffusion length is reached.

Reflection and recombination surfaces can be treated with the pseudo Monte Carlo approach described above by randomly assigning a reflection coefficient in accordance with the surface recombination velocity. This can be important for detectors at the boundary between the active layer and the substrate, which may be a partially reflecting surface to maximize optical response, and at the detector surface where there may be a high density of recombination sites due to incomplete surface passivation.

6. REACT Code Description

The general approach for the Radiation Environment Array Charge Transport (REACT) code is as follows: The device geometry is described by pixel pitch and layers (e.g., detector, ROIC, indium bump) on a Cartesian coordinate system. Depletion region and diffusion region thicknesses are defined and the boundary of regions within the pixel are defined. A particle is incident on the top surface of the device with a random location and random trajectory. The particle type and energy determine the linear energy transfer (LET) and thus the charge generation. A subarray (11 pixels x 11 pixels) is defined around the hit pixel. The particle traverses through the layers in a straight path and the appropriate charge collection model is applied, depending on the type of region – either depletion (high electric field), diffusion (low electric field), drift/diffusion (moderate electric field), or recombination (dead layer or recombination surface). Diffusion length is limited by recombination lifetime. The charge generated along the particle path is partitioned to the appropriate pixels in the subarray. The process is repeated for a large number of particles and the results accumulated in a large array (100 pixels x 100 pixels). The large array is of sufficient size to capture the statistical features of the interactions. A full image can be built up from stitching together multiple 100x100 arrays.

Fig. 4 shows the main screen. Charge collection to the 11x11 subarray is depicted by the three arrays on the left side, giving charge collected in the depletion layer (light blue), charge collected in the diffusion layer (light yellow) and total charge to the pixel (dark yellow) as the sum of depletion charge and diffusion charge. The input parameters for the current run are shown in the gray boxes in the center and right. The axes orientation and azimuth (phi) angle definitions are shown in the purple box. Definition of the offset parameters within a pixel is shown in the light green box. The current run parameters and run progress is given in the light blue boxes in the lower center. The dark green box provides hit rate calculations. The results of a run are displayed on the 100x100 array below the main page (not shown on the figure). A run is initiated by pressing the "Input" button, which brings up the graphical user interface (GUI) for inputting the run parameters. This interface is described in detail below. After the input parameters are loaded, the run is started by pressing the "Go" button. The results from each particle hit are shown in the subarray during the calculation and the distribution of the hits across the 100x100 array are displayed at the end of the calculation. The results can be plotted or cleared with the "Plot" or "Clear" buttons, respectively. The data in the 100x100 array can be analyzed and plotted as a histogram by pressing the "Histogram" button below the 100x100 array.

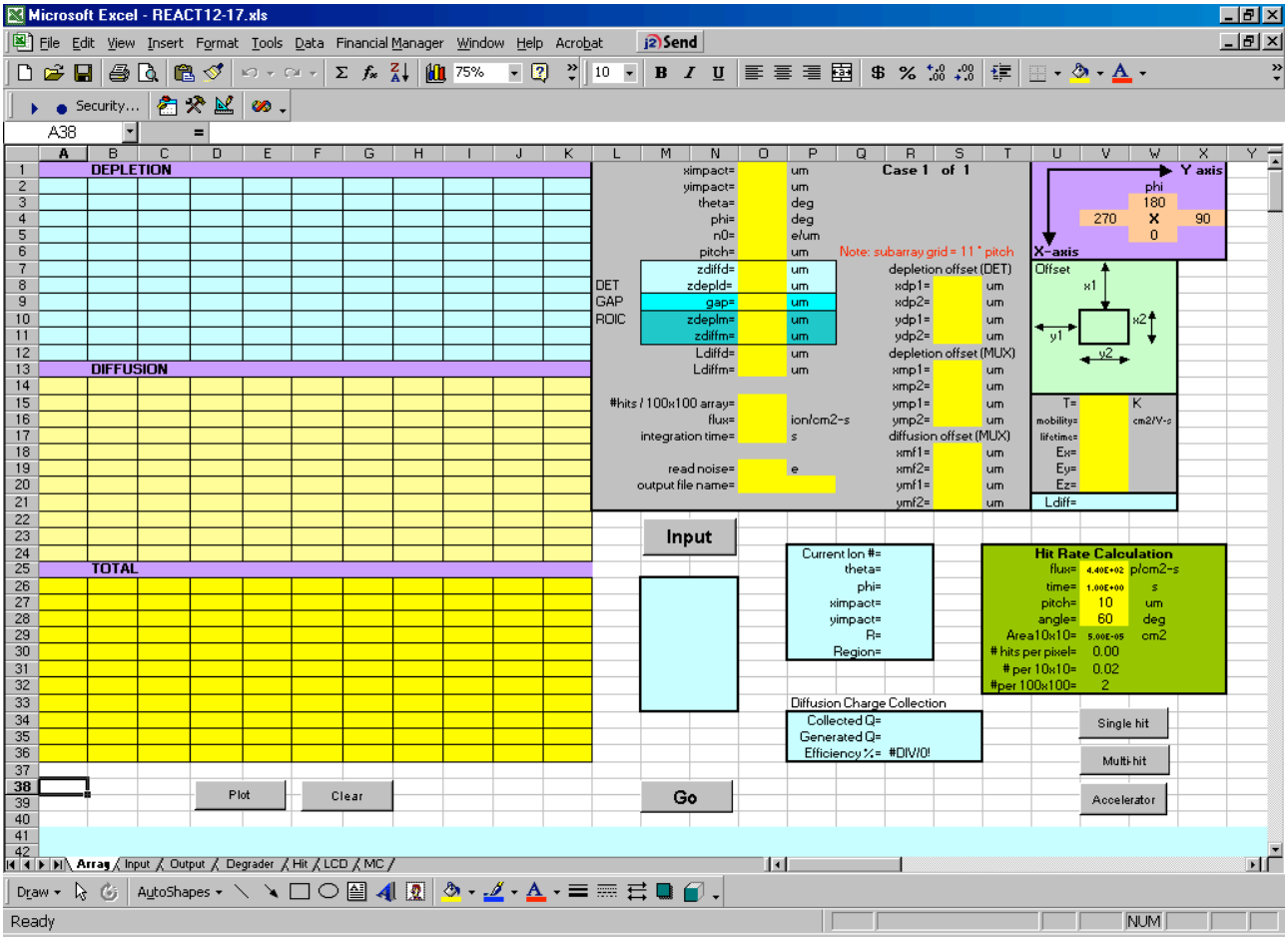

Figure 4. Main screen.

Fig. 5 shows the GUI input screen. Run control options are located along the top of the screen. The type of run can be “Single Run” or “Batch Run”, where several predefined cases are run in sequence. The type of device can be “ROIC”, “Detector” or “Hybrid”. The type of hit can be “Single Hit”, “Multi Hit” or “Accelerator Hit”. In “Single Hit”, the user defines the hit location (ximpact, yimpact) and trajectory (theta, phi). In “Multi Hit”, hit location and trajectory are randomly chosen. If the “Stacked” option is chosen in “Multi Hit”, multiple hits with random trajectory are stacked into the same hit location (pixel values combined and then divided by number of hits). In “Accelerator Hit”, the user defines the trajectory and the hit location is randomly chosen. The type of particle can be selected from “Specify LCD”, “Single Particle”, or “Hit File”. For “Specify LCD”, the user specifies the linear charge deposition (e/μm). For “Single Particle”, the user specifies the particle Z and energy, and the code calculates the LCD. For “Hit File”, the code randomly selects a particle from a list of particle cases in a hit file that is precomputed from a separate transport analysis. LET options include “Constant LET”, where there is no variation as the particle traverses the device, and “Vary LET”, where the code calculates the LET variation due to energy loss when traversing the device. Diffusion current model options include “Analytic Diffusion”, where an analytic diffusion model is used and “MC Diffusion”, where a Monte Carlo diffusion model is used. In the current implementation, the MC diffusion model is available for the Detector or ROIC, but not the Hybrid, due to the relatively long calculation time required. The GUI enables appropriate input boxes when the associated option is selected and disables and/or hides input boxes that are not appropriate for the chosen option.

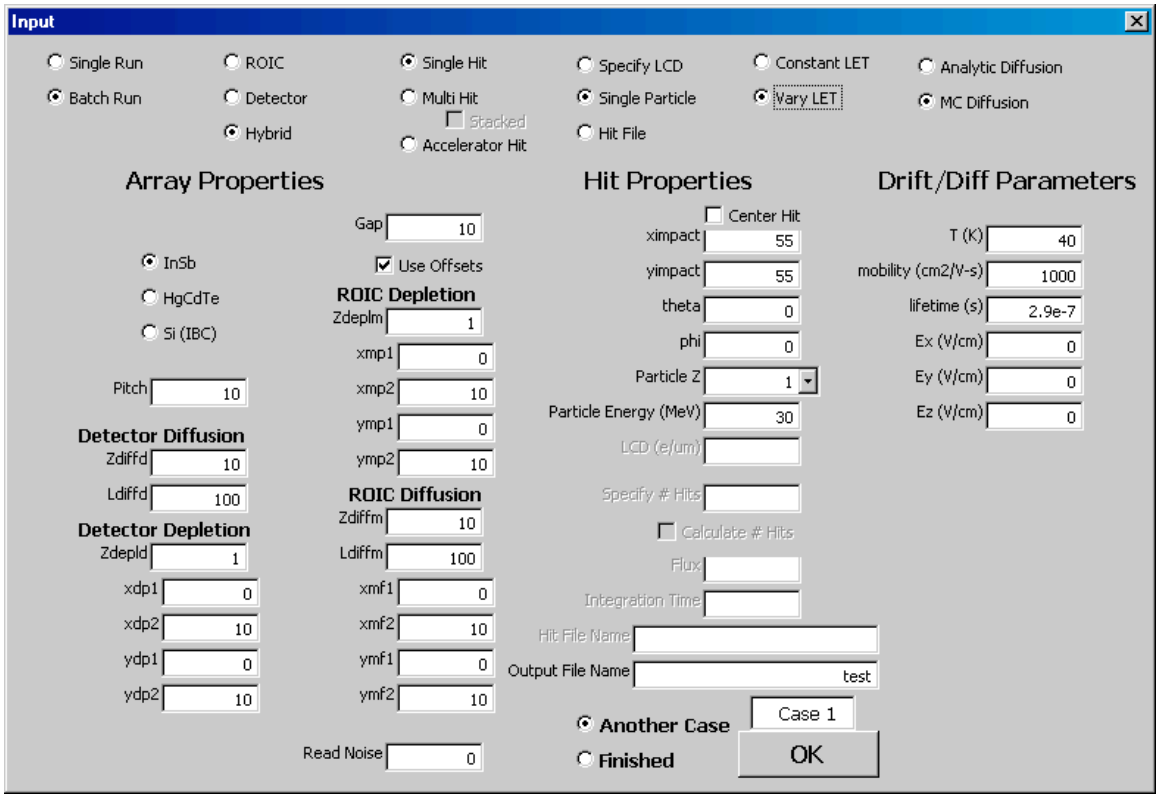

Figure 5. GUI input screen.

The lower part of the GUI screen is divided in sections related to array properties, hit properties and drift/diffusion model parameters. Under "Array Properties", the user can select detector types as InSb, HgCdTe or Si(IBC). The impact of the selection is on conversion of LCD to charge through the ionization energy, W. For InSb and HgCdTe, W is 1.5; for Si, W is 3.7. All dimensional parameters are in microns. Input parameters under "Array Properties" include pitch, gap between detector and ROIC, read noise (electrons) and geometric parameters for the detector and the ROIC. Detector parameters include detector diffusion width (Zdiffd), detector diffusion length (Ldiffd), detector depletion width (Zdepld) , and detector offset parameters (xdp1, xdp2, ydp1, ydp2). ROIC parameters include multiplexer depletion width (Zdeplm), multiplexer diffusion width (Zdiffm), multiplexer diffusion length (Ldiffm), multiplexer depletion region offset parameters (xmp1, xmp2, ymp1, ymp2), and multiplexer diffusion region offset parameters (xmf1, xmf2, ymf1, ymf2).

Under "Hit Properties", the user can define the hit location (ximpact, yimpact) and trajectory (theta, phi). Hit location is with respect to the 100x100 large array. The dimensions of the large array depend on pitch. For example if pitch = 10 μm, the large array has dimensions 1000 μm by 1000 μm. If the "Center Hit" option is chosen, the code centers the hit in the center pixel of the 11x11 subarray. The user can specify the LCD (e/μm) or can specify a particle Z (chosen from the drop-down option box) and energy (MeV). For the latter case, the code calculates the LCD. The user can either specify the number of hits or, if "Calculate # Hits" option is chosen, the code calculates the number of hits based on user inputs to "Flux" (p/cm^2-s) and "Integration Time" (s).

Under "Drift/Diff" Parameters", the user can input parameters for the drift/diffusion MC model as follows: temperature (K), minority carrier mobility (cm^2/V-s), minority carrier lifetime (s), and electric field (V/cm) vectors Ex, Ey, Ez.

At the bottom right of the screen, the path to the hit file (if not using the data provided on the workbook sheet "Hit") can be input by the user. The output file name and path can be input by the user. If the "Batch Run" option is chosen, the user has the option of "Another Case" or "Finished" when the "OK" button is selected. On selecting "OK" , the information on the GUI Sheet is transferred to the "Input Sheet" within the VB Application. When the code runs, the run parameters are read from the "Input Sheet" and transferred to the "Array Sheet".

Fig. 6 shows the overall code flow. The code is written in Visual Basic for Applications and is integrated with and runs under Excel as a spreadsheet application (REACT.xls). Table 3 lists the major forms, modules and functions and Table 4 lists the Workbook sheets.

After opening the Excel application (REACT.xls), the Array Sheet is displayed and the "Input" button can be selected to bring up the GUI Screen. After providing the input data for the run (or multiple runs in batch mode), selecting "OK" on the GUI transfers the run data to the Input Sheet. Upon selecting "Go", control is passed to the module "Control" which calls "Datadump" to transfer input data from the Input Sheet to the run parameter fields (yellow background within gray box) on the Array Sheet. "Control" also defines various parameters and flags to set up the conditions and parameters for the run. "LCD" calculates the charge generation rate (e/μm) based on the particle Z and current energy. The run is then passed to one of the three run options -- "Single Hit", "Multi Hit" or "Accelerator Hit". "Single Hit" runs one hit with hit location and trajectory defined by the user, "Multi Hit" runs multiple hits with random hit location on the large array and random trajectory and random particle Z and energy if the

"Hit File" option was selected. "Accelerator Hit" runs multiple hits with random hit location and fixed trajectory defined by the user.

For any of the three run options, the following series of events occurs: "Reset" resets variables and arrays, defines constants, and reads geometric properties of the device layers. "Clearsheet" clears previous data from Array Sheet. "Window" identifies the hit pixel based on the (x,y) hit location to the 100x100 large array and centers an 11x11 subarray around the hit pixel. The hit pixel is always (6,6) on the subarray. "Penetrate" tracks progress of the particle along a straight line path through the device layers. As charge is generated along the way in accordance with the current LCD (determined by module "LCD"), the charge is transported to the appropriate pixel in the subarray using the charge transport model appropriate for the current region ("Depletioncharge", Diffusioncharge", or Driftdiffusecharge"). The current pixel and the region (drift, diffusion or dead) are determined by "Navigate". The function QLSF provides the analytic solution to the diffusion equation. The module "Step" mechanizes a random walk calculation for the carriers generated by the penetrating particle. "Carriernavigate" provides the current location of the carriers as they move about under the influence of drift in the local field and diffusion. "Noise" generates random noise across the 100x100 array. "Saveit" saves the result to disk.

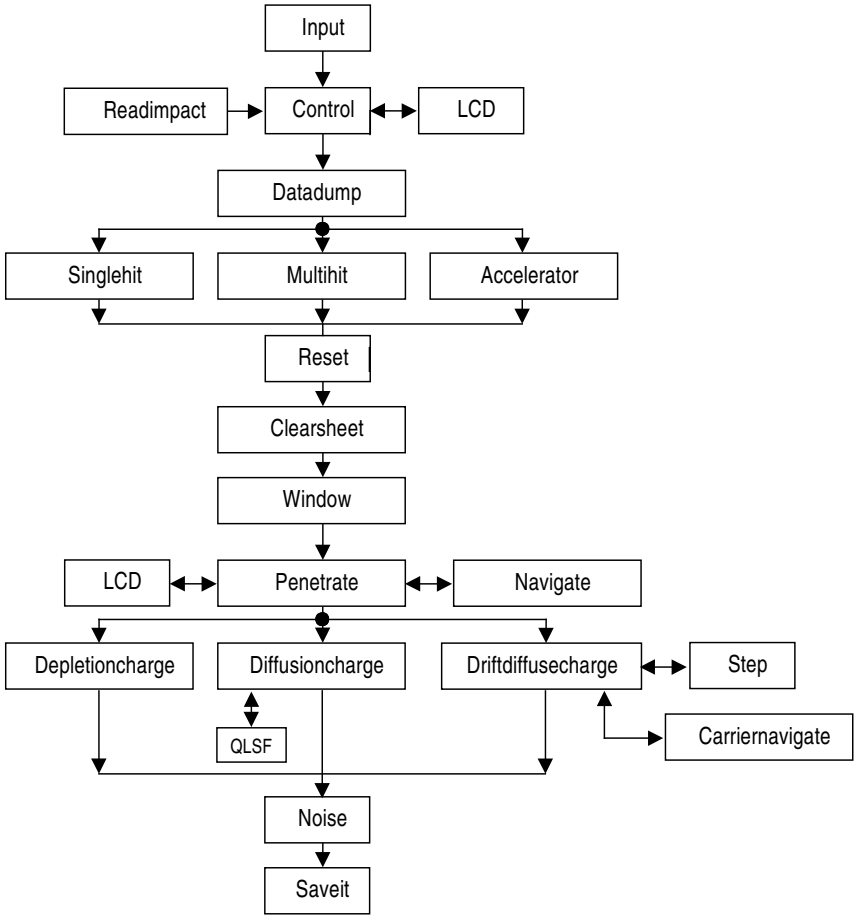

Figure 6. Major program modules and code flow.

Table 3. Code Forms, Modules and Functions

FORM	PURPOSE
Input1	Input form for setting up single runs or multiple runs in batch mode.
MODULE	PURPOSE
Control	Sets up the analysis based on flag values from Input1. Run parameters are stored on Input Sheet.
Datadump	Reads run parameters for current run from Input Sheet and writes to Array Sheet.
Readimpact	Randomly selects particle event from pre-computed hit file giving Z and energy.
Singlehit	Performs analysis for a single hit with hit location and angles defined by user.
Multihit	Performs analysis for specified number of hits with random hit location and random angles.
Accelerator	Performs analysis for specified number of hits with angles defined by user and random hit locations.
Reset	Resets arrays, defines constants, reads run parameters.
Clearsheet	Clears Array Sheet
Window	Identifies the hit pixel on 100x100 large array based on hit location and centers 11x11 subarray window around hit pixel.
Penetrate	Propagates particle through sample layers in straight line path. Charge is transported to appropriate pixel using model appropriate for the region.
Navigate	Called by Penetrate. Determines location of the particle along trajectory on xyz coordinates, determines the pixel for current location, determine type of region, and determines if there is an offset (depletion or well within pixel) from the pixel boundary.
Depletioncharge	Called by Penetrate. Determines charge generated in high-field region.
Diffusioncharge	Called by Penetrate. Determines charge generated in field-free region using analytical model for charge transport by diffusion.
Driftdiffusecharge	Called by Penetrate. Determines charge generated in low to medium field region using Monte-Carlo Model.
Step	Called by Driftdiffusecharge. Returns carrier location (x,y,z) due to diffusion step plus drift step.
Carriernavigate	Called by Driftdiffusecharge. Determines coordinates of pixel in which the carrier is currently located.
Noise	Generates random noise across 100x100 large array.
Saveit	Saves array results to disk.
Getit	Recalls array results from disk.
FUNCTION	PURPOSE
LCD	Called by Penetrate. Interpolates pre-computed TRIM data to get LET and calculates energy loss for particle for current trajectory increment.
QLSF	Called by Diffusioncharge. Returns incremental result based on analytic diffusion model.

Table 4. Workbook Sheets.

SHEET	DESCRIPTION
Array	Main page where program is started and intermediate results displayed.
Input	Stores run parameters.
Output	Displays completed run arrays and performs histogram analysis of the array data.
Degrader	Stores TRIM results for use in LET variation routines.
Hit	Stores pre-computed hit file data.
LCD	Utilities for LET calculation.
MC	Utilities for drift and diffusion parameter calculation.

7. Discussion

In this section we give example results, compare the analytic and Monte Carlo models for charge collection, discuss methods to extract model parameters from experimental data and compare model predictions to available experimental and space data.

7.1 Analytic Diffusion Model Example Results

Fig. 7 shows typical simulation results, using the analytic diffusion model, for charge collection from single ion hits. Charge collection in a 10x10 array of Si volumes with 1 µm depletion width, 20 µm diffusion width and 30 µm pitch is shown for two ion cases, 20 MeV proton and 200 MeV Fe. The ion hit is near the center of the array and the angle of incidence is 60 degrees, going from back to front in the picture. Charge is collected by drift in the depletion region of the hit pixel to give a peak. Charge is collected to adjacent pixels by diffusion.

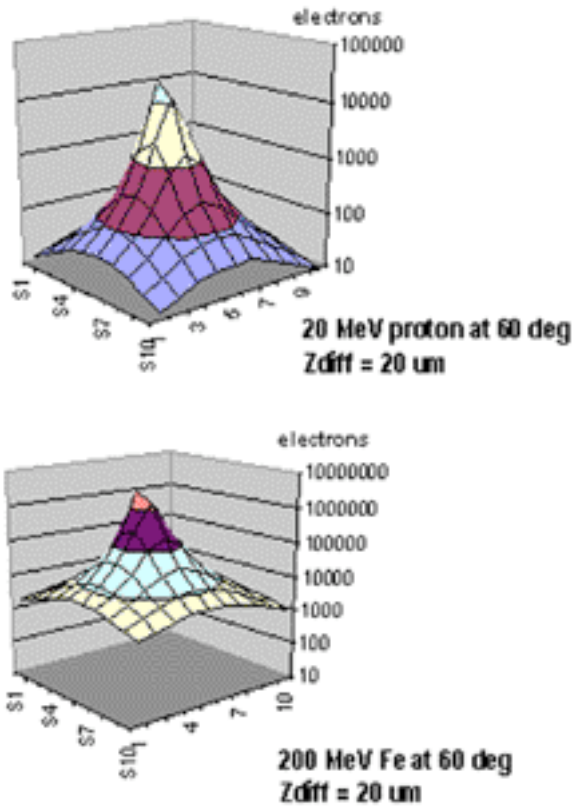

Figure 7. Charge collection in 10x10 array of Si pixels on 30 µm pitch with 1 µm depletion thickness and 10 µm diffusion thickness. Two ion cases are shown.

Fig. 8 shows analytic diffusion model results for the charge collected in individual pixels after a hit to a center pixel (5,5) of a 10x10 Si array with 30 µm pitch, 1 µm depletion thickness and 10 µm diffusion thickness. The particle is a 20 MeV proton incident at 80 degrees going from top to bottom in the picture. The top array shows the charge collected from the depletion region, the center array shows the charge collected from the diffusion region and the bottom array shows the total charge. Note the charge spread across the array, particularly in the pixels along the wake of the ion track. Depletion charge is collected only in the hit pixel. All of the other pixels are collecting charge by diffusion.

20 MeV proton at 80 deg, Zdiff = 10 um

0	0	0	0	0	0	0	0	0	0
0	0	0	0	0	0	0	0	0	0
0	0	0	0	0	0	0	0	0	0
0	0	0	0	0	0	0	0	0	0
0	0	0	0	7424	0	0	0	0	0
0	0	0	0	0	0	0	0	0	0
0	0	0	0	0	0	0	0	0	0
0	0	0	0	0	0	0	0	0	0
0	0	0	0	0	0	0	0	0	0
0	0	0	0	0	0	0	0	0	0

DEPLETION

7	8	11	12	13	12	10	8	6	5
9	13	18	23	24	22	18	13	9	7
14	22	34	49	56	48	33	21	14	9
20	36	70	137	195	135	68	35	19	11
26	55	145	585	20881	550	140	54	25	14
30	71	236	1814	30406	1643	225	69	30	15
30	70	229	1656	13432	1510	218	68	29	15
25	53	132	416	882	399	127	51	25	14
19	33	62	111	142	109	61	33	18	11
13	20	31	42	48	42	30	20	13	8

DIFFUSION

7	8	11	12	13	12	10	8	6	5
9	13	18	23	24	22	18	13	9	7
14	22	34	49	56	48	33	21	14	9
20	36	70	137	195	135	68	35	19	11
26	55	145	585	28305	550	140	54	25	14
30	71	236	1814	30406	1643	225	69	30	15
30	70	229	1656	13432	1510	218	68	29	15
25	53	132	416	882	399	127	51	25	14
19	33	62	111	142	109	61	33	18	11
13	20	31	42	48	42	30	20	13	8

TOTAL

Figure 8. Charge collected in depletion and diffusion arrays is combined for the total charge array. Charge to the hit pixel is collected by drift and charge to other pixels is collected by diffusion.

Fig. 9 shows analytic model predictions of crosstalk to the nearest neighboring pixels for the case of a 30 µm pitch Si pixel struck in the center with an ion at normal incidence. Crosstalk is a function of both pitch and diffusion layer thickness. When omni directional hits and random hits within the pixel area are considered, the crosstalk is larger.

Fig. 10 illustrates the model output with a plot of 200 ion hits representative of a GCR spectrum on a 100x100 HgCdTe array with 20 µm pitch. The analytic diffusion model was used. Also shown is the pulse height distribution calculated from the "Histogram" selection button on Array Sheet.

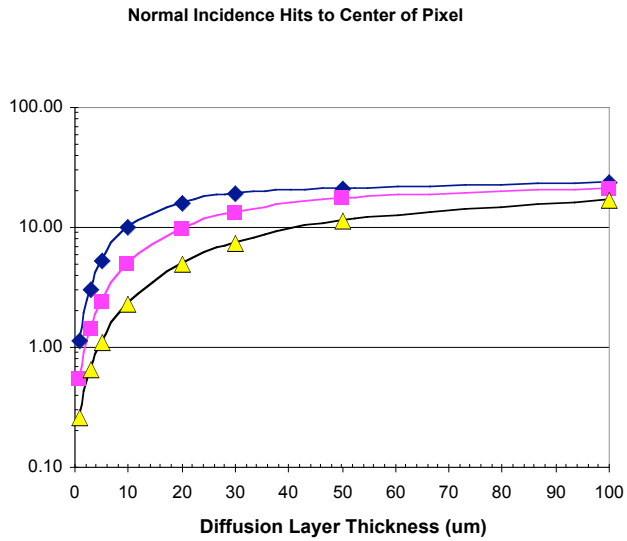

Figure 9. Model predictions of crosstalk as a function of diffusion layer thickness and pixel pitch.

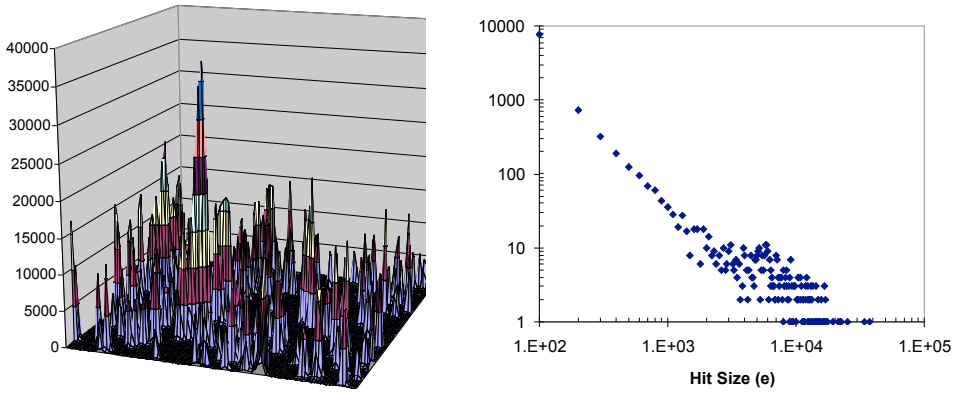

Figure 10. Example result for 100 pixel x 100 pixel array with 20 μm pitch.

7.2 Monte Carlo Drift/Diffuse Model Example Results

Fig. 11 shows Monte Carlo (MC) model predictions for the drift step versus electric field. For this example, the drift correction is relatively small below 100 V/cm, and using the analytic solution to the diffusion equation is appropriate. Above 1E5 V/cm, the drift step dominates and it is appropriate to apply the drift model and assume all charge is collected. In the intermediate region, the MC model gives the result. Similar analysis should be done for actual cases to determine the requirement of using the MC approach vice the analytic approach.

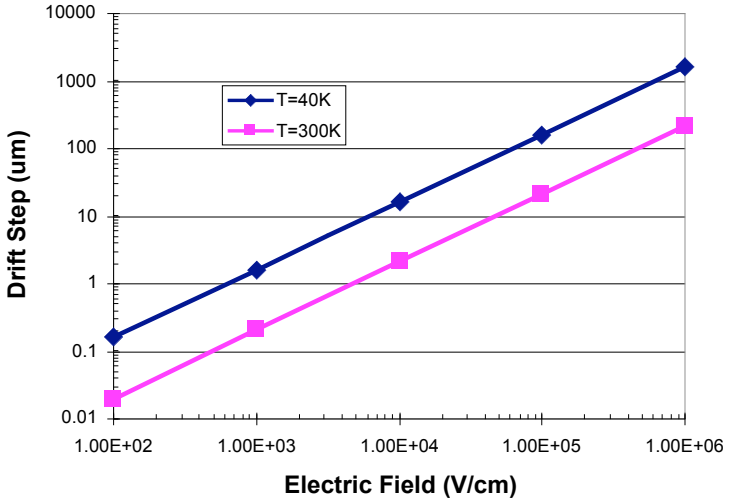

Figure 11. Drift step versus electric field.

Fig. 12 compares drift step to diffusion step for 3 values of electric field. In the actual application of the model, the diffusion step is limited by the diffusion length.

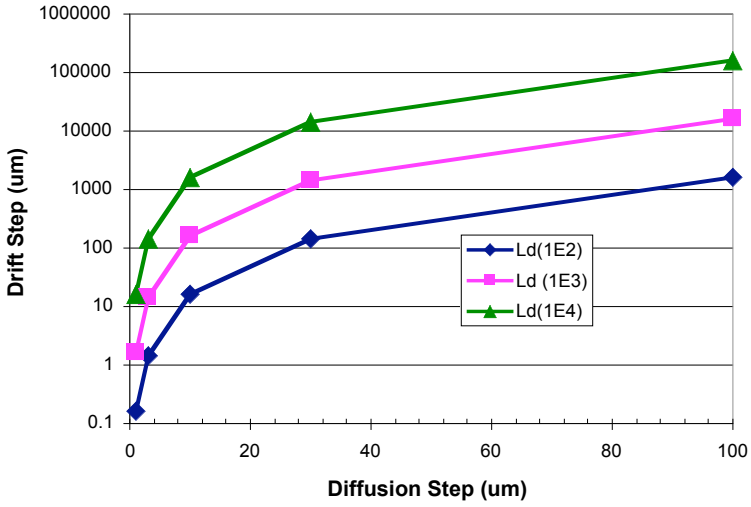

Figure 12. Drift step versus diffusion step for various electric fields.

Fig. 13 illustrates MC model predictions for movement of 100 particles by diffusion and drift for cases of zero field, 100 V/cm and 500 V/cm. The electric field direction is “up” in the figure. The field-assisted drift imposed on the diffusion process is evident.

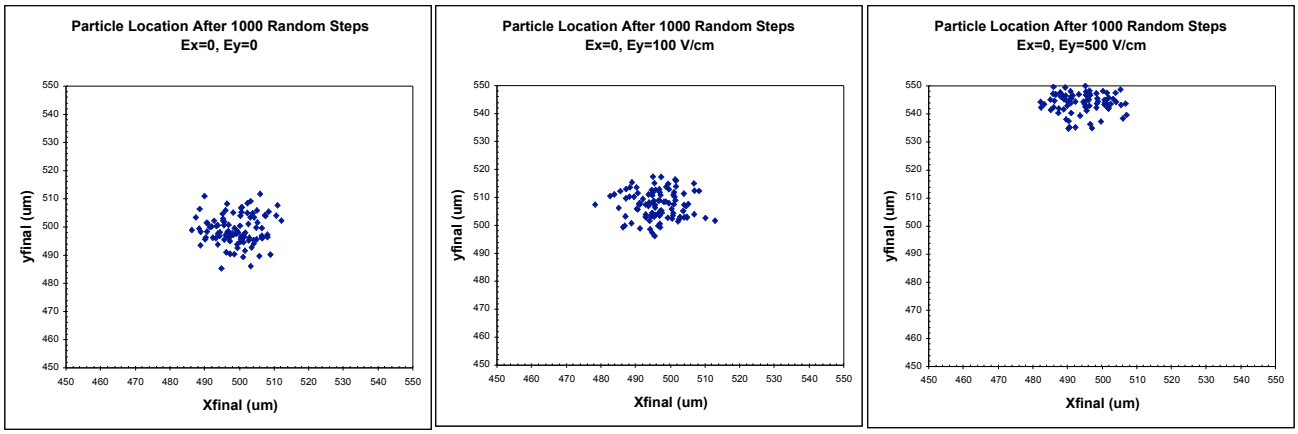

Figure 13. Particle movement by drift and diffusion with electric field of 0, 100, and 500 V/cm. Final location is shown for 100 particles. Particles begin at (500,500).

Fig. 14 compares charge spread in an 11x11 pixel subarray with various pitch for the analytic (left side) and the MC (right side) diffusion models. The ion hit is normal incidence with LCD of 1000 e/μm and centered on pixel (6,6), the center of the subarray. A Si structure with 1 μm depletion thickness and 10 μm diffusion thickness is modeled. The MC model parameters were chosen to give a diffusion length of 10 μm (T = 40 K, mobility = 1000 V-cm^2/s, lifetime = 290 ns).

We note generally good agreement between the two models for diffusion. The center (peak) regions agree better at larger pitch and the edge regions agree better at smaller pitch. The total collected charge is about the same for the two models in each case.

Fig. 15 illustrates the effect of electric field on charge collection. Using the same ion hit, subarray and device parameters as shown in Fig. 14, we show charge collection in an 11x11 array for different electric fields in the y-direction. Results are shown for Ey of 0, 10, 100 and 1000 V/cm. Ex = Ez = 0 for all cases. The peak at the center location (6,6) is unaffected by the field in the diffusion region since it is due to the depletion region where the field is assumed to dominate and collect all of the charge generated in the region. We note observable influence on diffusion charge at even 10 V/cm as there is no charge collected in the pixels near the y = 0 origin since it is pushed by the drift field in the y-direction. At 1000 V/cm, most of the charge generated in the diffusion region is moved across and off the array by drift in the electric field before reaching the depletion boundary.

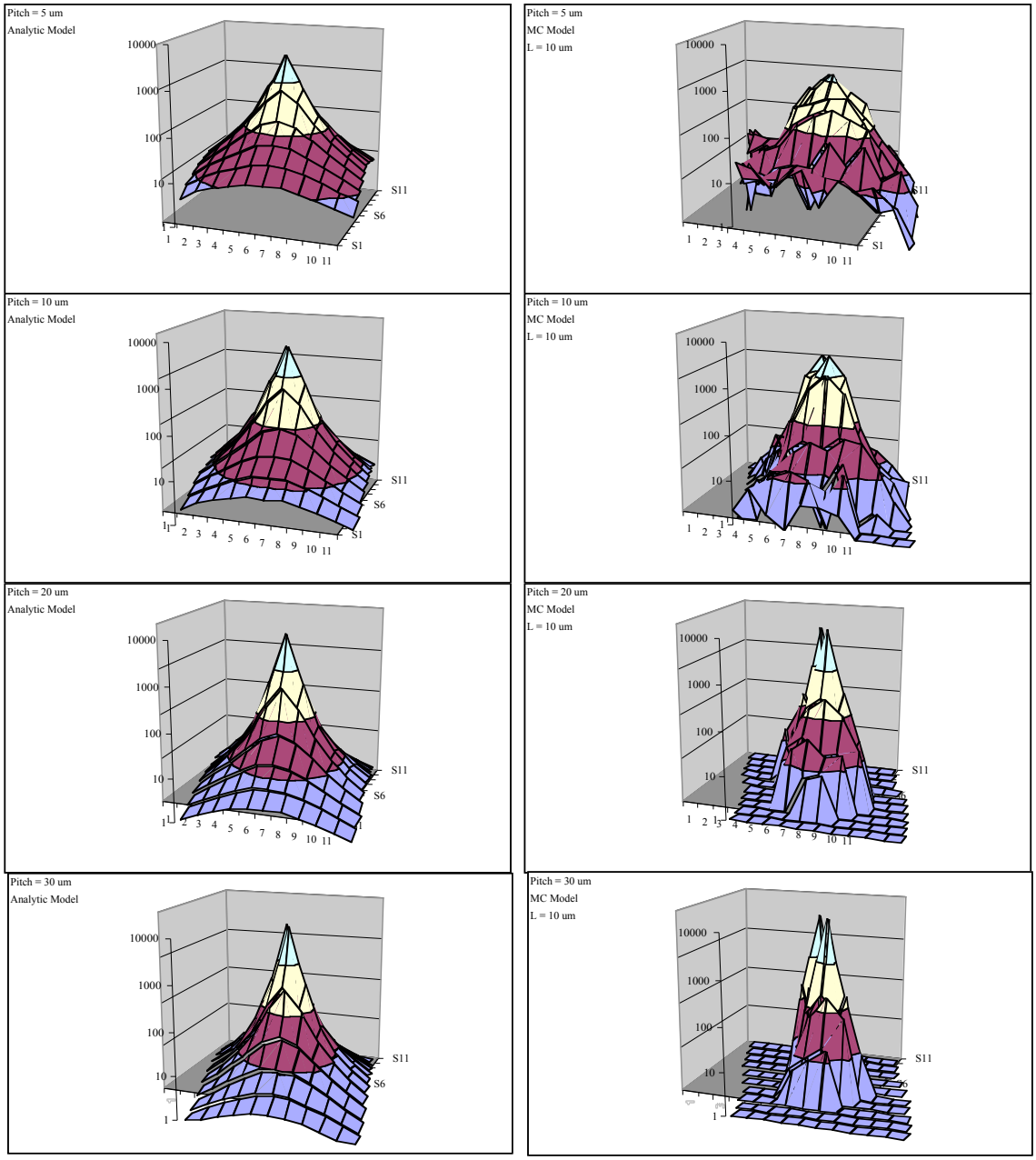

Figure 14. Comparison of charge spread with analytic diffusion model and Monte Carlo diffusion model for an 11x11 array with various pitch.

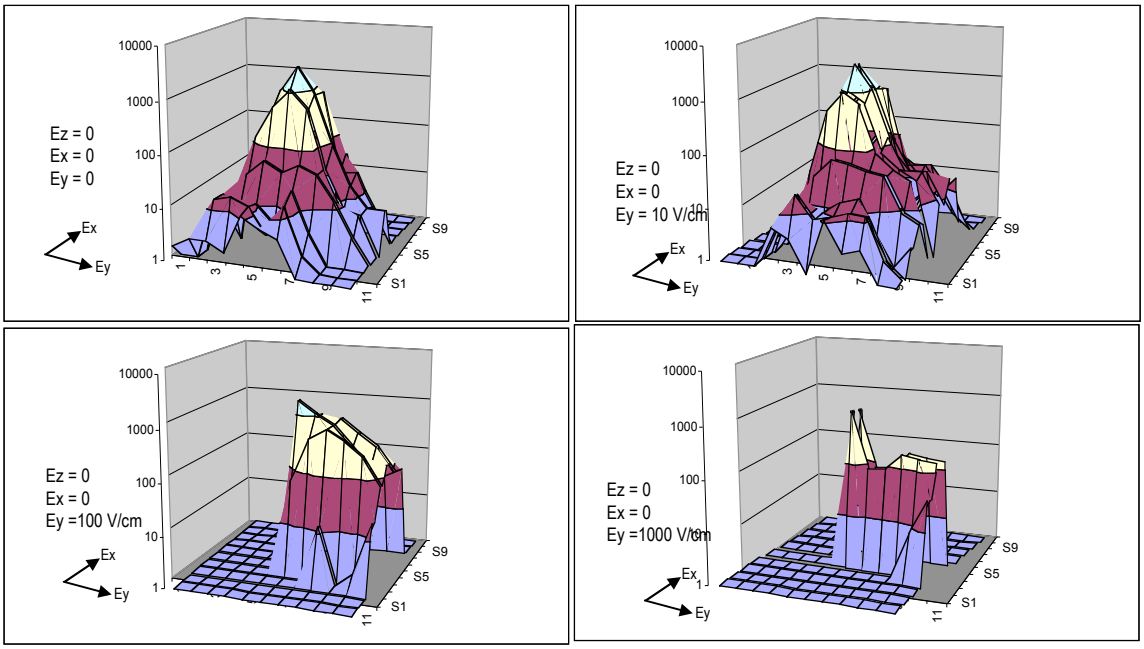

Figure 15. Charge spread from a normal incidence hit to center pixel in 11x11 array with various electric fields in the y-direction.

Fig. 16 shows the same case as Fig. 15 except the electric field is directed in the x-direction (toward the bottom in the figure). Ex is varied and Ey = Ez =0. Again we note the drift assisted diffusion toward the field direction, with the depletion peak unaffected.

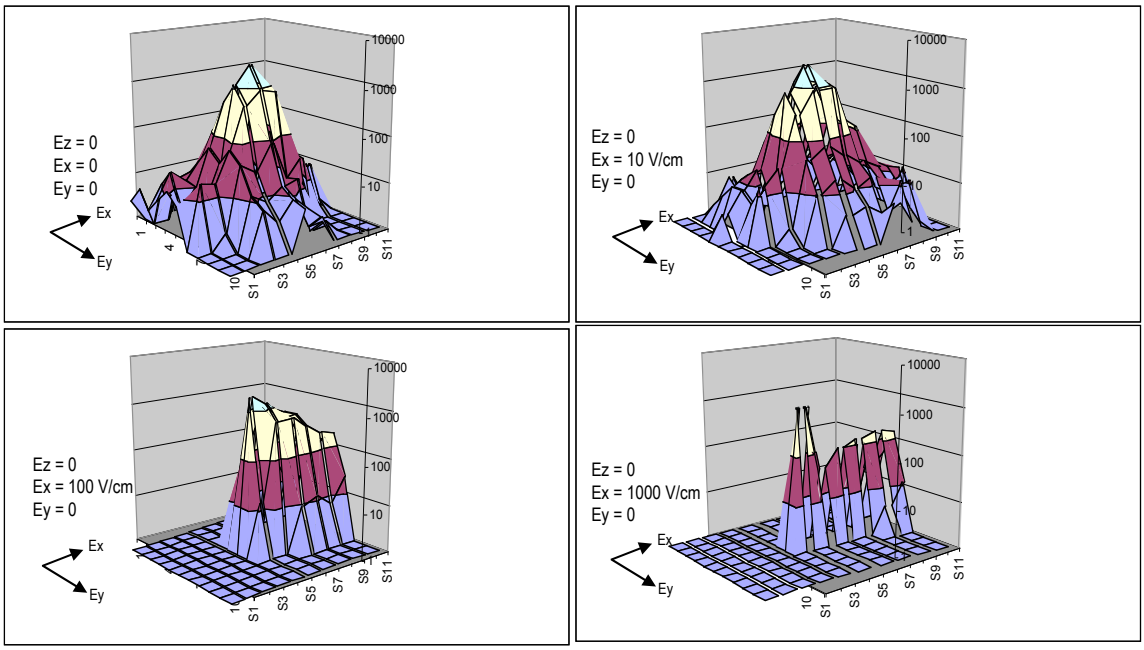

Figure 16. Charge spread from a normal incidence hit to center pixel in 11x11 array with various electric fields in the x-direction.

Fig. 17 shows the effects of a vertical electric field (Ez) on charge spread in an array with the same parameters as Figures 15 and 16. A negative electric field is in the direction toward the depletion boundary; a positive field is in the direction away from the depletion boundary. For the top sub-figure, the negative field causes all of the generated charge to be captured. For the lower sub-figures, the electric field pushes the charge away from the depletion boundary. Note that a field of only 100 V/cm is sufficient to push most of the charge generated in the diffusion region away from the depletion boundary.

Ez=-100 Negative field pushes charge toward depletion boundary

0	0	0	0	0	0	0	0	0	0	0
0	0	0	0	0	0	0	0	0	0	0
0	0	0	0	0	0	0	0	0	0	0
0	0	0	0	0	0	0	0	0	0	0
0	0	0	0	578	1247	678	0	0	0	0
0	0	0	0	1341	3455	1121	0	0	0	0
0	0	0	0	624	1263	693	0	0	0	0
0	0	0	0	0	0	0	0	0	0	0
0	0	0	0	0	0	0	0	0	0	0
0	0	0	0	0	0	0	0	0	0	0
0	0	0	0	0	0	0	0	0	0	0

Ez=10 Positive field pushes charge away from depletion boundary

0	0	0	0	1	0	0	0	0	0	0
0	1	17	3	10	3	6	2	8	1	0
0	13	5	7	9	17	0	12	16	0	0
0	0	9	6	33	53	26	23	10	1	0
0	0	6	30	445	928	284	21	10	4	1
0	2	6	43	795	2492	796	64	8	4	0
0	2	8	36	581	677	507	13	13	4	0
0	4	6	4	49	50	5	11	11	0	0
0	2	0	0	11	9	0	0	1	0	0
0	0	0	0	0	0	0	0	0	0	0
0	0	0	0	0	0	0	0	0	0	0

Ez=100 Note that essentially all diffusion from 10 um layer is stopped by only 100 V/cm i.e., 0.1 V/10 um

0	0	0	0	0	0	0	0	0	0	0
0	0	0	0	0	0	0	0	0	0	0
0	0	0	0	0	0	0	0	0	0	0
0	0	0	0	0	0	0	0	0	0	0
0	0	0	0	0	0	0	0	0	0	0
0	0	0	0	0	1374	0	0	0	0	0
0	0	0	0	0	0	0	0	0	0	0
0	0	0	0	0	0	0	0	0	0	0
0	0	0	0	0	0	0	0	0	0	0
0	0	0	0	0	0	0	0	0	0	0
0	0	0	0	0	0	0	0	0	0	0

Ez=1000

0	0	0	0	0	0	0	0	0	0	0
0	0	0	0	0	0	0	0	0	0	0
0	0	0	0	0	0	0	0	0	0	0
0	0	0	0	0	0	0	0	0	0	0
0	0	0	0	0	0	0	0	0	0	0
0	0	0	0	0	1000	0	0	0	0	0
0	0	0	0	0	0	0	0	0	0	0
0	0	0	0	0	0	0	0	0	0	0
0	0	0	0	0	0	0	0	0	0	0
0	0	0	0	0	0	0	0	0	0	0
0	0	0	0	0	0	0	0	0	0	0

Figure 17. Effect of vertical electric field (Ez) on charge spread in 11x11 array.

7.3 Calibration of Model Parameters

The model contains many adjustable parameters, and it is important to calibrate these parameters with experimental data. Because the secondary particle environment is strongly dependent on the exact material and geometric configuration around the "flight" FPA and the primary particle spectrum on-orbit, it is generally not practical to test for the secondary environment. Our strategy is to calibrate the models with the primary particles and extrapolate the effects of the secondary environment with the calibrated models and detailed transport analysis. A key advantage of detailed modeling and simulation tools as described here, over simpler models that merely account for average behavior, is that aggregate behavior for a large number of hits can be studied in statistically significant quantities. These results can then be compared to measured data from space, and to controlled experiments at ground-based accelerator testing to calibrate model parameters.

Studying pulse height distribution is one method of comparing model results to experiment and inferring model parameter values. The maximum and average charge pulses in the distribution are related to the maximum and average pathlength, respectively, in the charge collection volume, which in turn are related to the geometry of the collection volume. Fig. 18 shows pulse height distribution simulation results for a 100x100 pixel HgCdTe detector array with 20 µm pitch, 1 µm depletion layer and different diffusion layer thicknesses. The particle LCD is constant at 1000 e/µm, consistent with GeV range protons in 5 µm cutoff HgCdTe. The simulation is for 300 hits, randomly located and with random trajectory, as would be the case for exposure in space. The high end of the distribution is due to the primary hits and the low end of the distribution is due to charge spread (crosstalk) to neighboring pixels. The average pulse amplitude and maximum pulse amplitudes for the primary hits are consistent with expectations from simple models that calculate average and maximum pathlength in a rectangular parallelepiped.

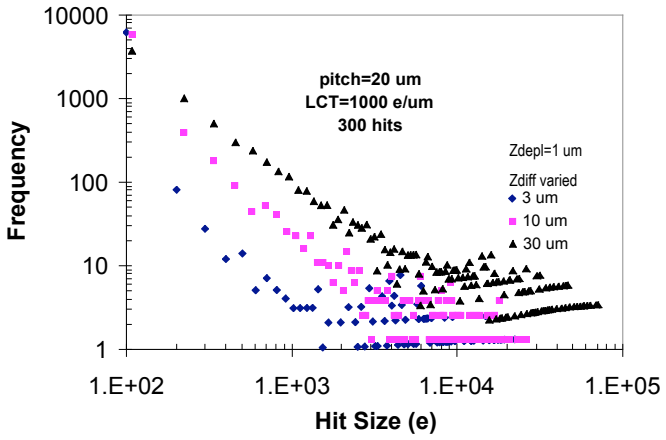

Figure 18. Pulse height distribution simulation results for 300 hits to 20 µm pitch, 100x100 array of HgCdTe detectors. The particles simulate GeV-range protons with omni directional incidence.

Fig. 19 shows pulse height distributions for simulation of 30 MeV proton hits to HgCdTe detectors with the same pitch and layer thicknesses as discussed in Fig.10. In this case, we are simulating an accelerator test and have 100 proton hits randomly located across the 100x100 array but all with 60 degree incidence. Note the different slopes of the distribution in the lower energy tails. The slope decreases with increasing diffusion layer thickness. Such simulation information can be combined with test data to infer an effective diffusion layer thickness.

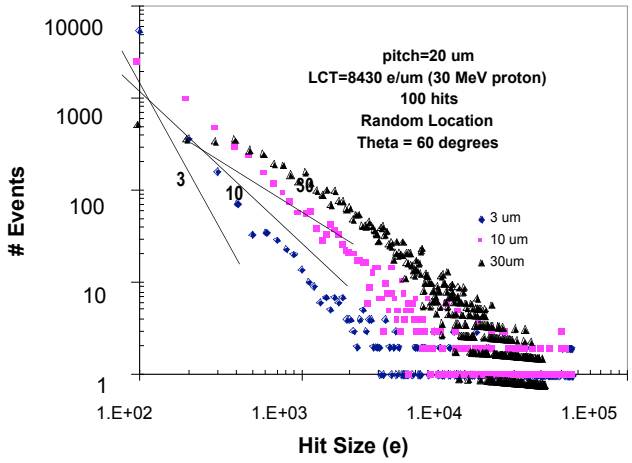

Figure 19. Pulse height distribution simulation results for 100 hits to 20 µm pitch, 100x100 array of HgCdTe detectors. The particles simulate 30 MeV protons with 60 degree angle of incidence.

7.4 Comparison to Measured Data

The original plan was to use cyclotron test data from the JWST program to calibrate and validate the models. However, delays in development of the FPA components from the competing JWST FPA vendors delayed the testing, and therefore the data was not available for this report. Alternatively, we have used available data to begin model calibration and validation as discussed below. The JWST experimental program is ongoing and as test data becomes available, the model will be evaluated against the data and refined as required.

7.4.1 NICMOS On-Orbit Data

After considerable data processing and interpretation, on-orbit data from a HgCdTe FPA in the NICMOS camera on the Hubble Space Telescope provides a rich data source for cosmic ray induced transients [13]. Fig. 20 shows an observed pulse height distribution from dark field images from NICMOS taken outside of the South Atlantic Anomaly (SAA).

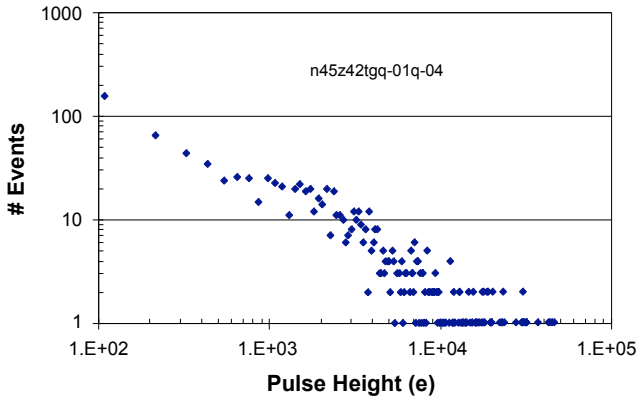

Figure 20. Pulse height distribution observed on-orbit for NICMOS (after data processing).

The NICMOS environment outside of SAA consists mostly of GeV-range protons. The magnetosphere has filtered out lower energy particles, leaving a nearly mono-LET source of omni directional protons with LCD of ~1200 e/um in the HgCdTe detector array. See Reference 13 for details.

Fig. 21 shows model simulation of the pulse height distribution for the NICMOS conditions shown in Fig 20. The simulation assumes a 40 um pitch with a 1 um depletion layer thickness and a 5 um diffusion layer thickness. The results are for 300 primary hits, using the analytic diffusion model. Secondary particles are not included in the simulation. The LCD is 1200 e/um and hits are random in location and trajectory. The larger pulses in the spectrum are due to the primary hits. The lower energy tail is due to crosstalk. We see good agreement on the primary particle hit amplitudes and general qualitative agreement on the shape of the distribution. There are more low amplitude pulses in the simulation than were observed in the data.

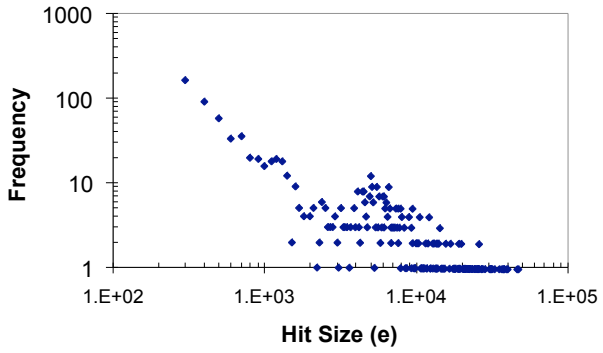

Figure 21. Model prediction for NICMOS pulse height distribution. The distribution includes 300 primary hits with random location and trajectory on a 100x100 array.

7.4.2 Active Pixel Sensor Test Chip Cyclotron Data

Heavy ion tests on an Active Pixel Sensor (APS) test chip also provide a source of data for validating the charge collection aspects of the model [14]. In Fig. 22, we compare model simulations using the analytic diffusion model to test data for 600 MeV Ar hits to an APS test chip. The APS test chip is a 256x256 Si photodiode array and is separated into 4 quadrants of 128x128 pixels [15]. The pixel pitch is 16.2 µm. Each quadrant has a different pixel design that affects the charge collection characteristics. Consequently there was large variation in the response to heavy ion hits for each of the quadrants [14]. We show test data for a 600 MeV Ar hit to quadrant 1 (left figure) and quadrant 2 (middle figure). The data saturates at 1700 DN (digital number) counts. The simulation is shown as the right figure, with artificial saturation imposed at 1700 DN. The simulation assumed a 1 µm depletion layer thickness and 25 µm diffusion layer thickness, with both layers covering the entire pixel area. In both the data plots and the simulation plot, an 11x11 array is centered around the ion hit at normal incidence.

Qualitatively, the simulation results are intermediate between the quadrant 1 and quadrant 4 data. We see general agreement on the gross characteristics of the charge spread. Compared to the simulation, quadrant 1 has a more focused charge collection and quadrant 2 has a less focused charge collection. The actual charge collection volumes within the pixel are much more complex than the simple depletion layer on a diffusion layer that was assumed for the simulation, and the electric fields within the structure probably modify the diffusion characteristics beyond the simple free-field diffusion assumed in this simulation. The intent of this analysis was to reproduce the gross features of the data. A more comprehensive analysis that takes the detailed pixel charge collection structures and internal electric fields into account will be performed in the future.

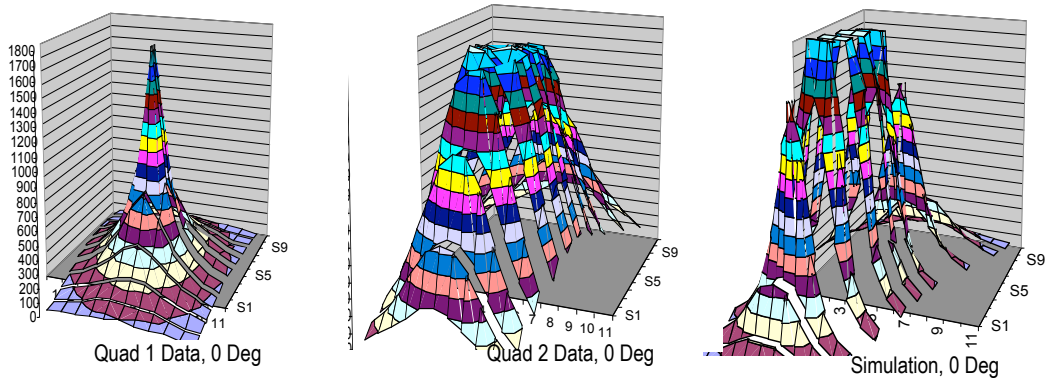

Figure 22. Ar ion hits at 0 degrees on 2 quadrants of Active Pixel Sensor test chip compared to model simulation.

8. Summary

We have developed charge collection models and a structured approach for simulating ionizing particle interactions with detector arrays. The modeling uses a combination of analytical and Monte Carlo techniques to capture the essential features of charge collection to the detector pixels. The model addresses several aspects that are necessary for high fidelity simulation of complex FPA structures including multiple layers, sub-regions within layers, variation of LET with range, secondary electron scattering, free-field diffusion, and field-assisted diffusion.

The models were integrated into a computer code, REACT, that serves as an engineering tool to predict charge collection in an array of collection elements. Methodology for calibration of model parameters with experimental data were discussed, and comparison of simulation predictions to available data was presented. The REACT code will be refined as cyclotron test data on FPA components becomes available on the JWST program.

The modeling approaches were presented at the IEEE Aerospace Conference, the Single Event Effects Symposium and the IEEE Nuclear and Space Radiation Effects Conference.

While the modeling and code development have concentrated on infrared detector arrays, the simulation methodology and modeling tools can be applied to any semiconductor detector array to predict radiation-induced charge collection.

References

[1] J.C.Pickel, R.A.Reed, R.Ladbury, B.Rauscher, P.W.Marshall, T.M.Jordan, B.Fodness and G.Gee, "Radiation-Induced Charge Collection in Infrared Detector Arrays," accepted for publication in IEEE Transactions on Nuclear Science, Dec. 2002.

[2] A.Fowler, T.Greene, M.Greenhouse, D.Hall, K.Long, J.MacKentry, B.Martineau, C.McCreight, J.Pipher, M Ressler and E.Young, "Recommendations of the NGST Detector Requirements Panel," NGST Document 641, October, 1999.

[3] J.C.Pickel, R.Reed, R.Ladbury, B.Rauscher, P.Marshall, T.Jordan, B.Fodness and G.Gee, "Modeling Radiation-Induced Transients in the Next Generation Space Telescope (NGST)," 2002 IEEE Aerospace Conference, March 2002.

[4] Offenberg et al. 1999, "Cosmic Ray Rejection Aboard the NGST," in ASP Conference Series, "Astronomical Data Analysis Systems and Software VIII," in press.

[5] J.L.Barth, J.C. Isaacs, and C. Poivey, "The Radiation Environment for the Next Generation Space Telescope," NGST Document 570, September 2000.

[6] A.Claret, H.Dzitko and J.J.Engelmann, "Transient Particle Effects on the ISOCAM Instrument On-Board the Infrared Space Observatory," IEEE Trans. Nucl. Sci., Vol. 49, No. 6, p. 1511, December 1999.

[7] T.S.Lomheim, R.M.Shima, J.R.Angione, W.F.Woodward, D.J.Asman, R.A.Keller and L.W.Schumann, "Imaging Charge-Coupled Device (CCD) Transient Response to 17 and 50 MeV Proton and Heavy Ion Irradiation," IEEE Trans. Nucl. Sci., Vol. 37, No. 6, p. 1876, December 1990.

[8] T.E.Dutton, W.F.Woodward and T.S.Lomheim, "Simulation of Proton-Induced transients on Visible and Infrared Focal Plane Arrays in a Space Environment, SPIE, Vol. 3063, p.77, 1997.

[9] J.F.Ziegler, J.P.Biersack and U.Littmark, "The Stopping and Range of Ions in Solids," Pergamon Press, 1985.

[10] T.M.Jordan, "An Adjoint Charged Particle Transport Method," IEEE Trans. Nucl. Sci., Vol. 23, 1976.

[11] S.Kirkpatrick, "Modeling Diffusion and Collection of Charge from Ionizing Radiation in Silicon Devices," IEEE Trans. Elec. Dev., Vol. ED-26, p. 1742, 1979.

[12] G.A.Sai-Halasz and M.R.Wordeman, "Monte Carlo Modeling of the Transport of Ionizing Radiation Created Carriers in Integrated Circuits," IEEE Elect. Dev. Lett., Vol. EDL-1, No. 10, p. 211, October 1980.

[13] R.Ladbury, J.C.Pickel, G.Gee, T.M.Jordan, L.Bergeron, B.Raushcer, R.A.Reed, P.W.Marshall, D.Figer and B.Fodness, "Characteristics of the Hubble Space Telescope's Secondary Radiation Environment Inferred from Charge Collection Modeling of Near Infrared Camera and Multi-Object Spectrometer," 2002 NSREC.

[14] P.W.Marshall, W.B.Byers, C.Conger, E.Eid, G.Gee, M.R.Jones, C.J.Marshall, R.A.Reed, J.C.Pickel, S.Kniffen and J.Peden, "Heavy Ion Transient Characterization of a Photobit Hardened-by-Design Active Pixel Sensor Array," 2002 NSREC.

[15] E.S.Eid, T.Y.Chan, E.R.Fossum, R.H.Tsai, R.Spagnuolo, J.Deily, W.B.Byers,Jr. and J.Peden, "Design and Characterization of Ionizing Radiation-Tolerant CMOS APS Image Sensors up to 30 Mrd(Si) Total Dose," IEEE Trans. Nucl. Sci., Vol. 48, No. 6, p. 1796, December 2001.

REPORT DOCUMENTATION PAGE

Form Approved
OMB No. 0704-0188

1. AGENCY USE ONLY *(Leave Blank)*	2. REPORT DATE	3. REPORT TYPE AND DATES COVERED
	June 2003	Contractor Report

4. TITLE AND SUBTITLE

Modeling Charge Collection in Detector Arrays

5. FUNDING NUMBERS

H–32491D

6. AUTHORS

J.C. Pickel

7. PERFORMING ORGANIZATION NAMES(S) AND ADDRESS(ES)

PR&T, Inc.
P.O. Box 1474
Bonsall, CA 92003–1474

8. PERFORMING ORGANIZATION REPORT NUMBER

M–1079

9. SPONSORING/MONITORING AGENCY NAME(S) AND ADDRESS(ES)

NASA's Space Environments and Effects (SEE) Program
George C. Marshall Space Flight Center
Marshall Space Flight Center, AL 35812

10. SPONSORING/MONITORING AGENCY REPORT NUMBER

NASA/CR—2003–212504

11. SUPPLEMENTARY NOTES

Prepared for NASA's Space Environments and Effects (SEE) Program by PR&T, Inc.
Technical Monitor: Donna Hardage, NASA Marshall Space Flight Center, 256–544–2342

12a. DISTRIBUTION/AVAILABILITY STATEMENT

Unclassified-Unlimited
Subject Category 93
Standard Distribution

12b. DISTRIBUTION CODE

13. ABSTRACT *(Maximum 200 words)*

A detector array charge collection model has been developed for use as an engineering tool to aid in the design of optical sensor missions for operation in the space radiation environment. This model is an enhancement of the prototype array charge collection model that was developed for the NGST program. The primary enhancements were accounting for drift-assisted diffusion by Monte Carlo modeling techniques and implementing the modeling approaches in a windows-based code. The modeling is concerned with integrated charge collection within discrete pixels in the focal plane array (FPA), with high fidelity spatial resolution. It is applicable to all detector geometries including monolithic charge coupled devices (CCDs), Active Pixel Sensors (APS) and hybrid FPA geometries based on a detector array bump-bonded to a readout integrated circuit (ROIC).

14. SUBJECT TERMS

radiation, FPA, CCD, detector, arrays, ionizing, Monte Carlo, transport, LET, charge, drift, diffusion

15. NUMBER OF PAGES

38

16. PRICE CODE

17. SECURITY CLASSIFICATION OF REPORT	18. SECURITY CLASSIFICATION OF THIS PAGE	19. SECURITY CLASSIFICATION OF ABSTRACT	20. LIMITATION OF ABSTRACT
Unclassified	Unclassified	Unclassified	Unlimited